

Improved excitation mode selectivity of high- T_c superconducting terahertz emitters

Kashiwagi, Takanari; Yuasa, Takumi; Tanabe, Yuki; Imai, Takayuki; Kuwano, Genki; Ota, Ryusei; Nakamura, Kento; Ono, Yukino; Kaneko, Youta; Tsujimoto, Manabu

DOI

[10.1063/1.5033914](https://doi.org/10.1063/1.5033914)

Publication date

2018

Document Version

Final published version

Published in

Journal of Applied Physics

Citation (APA)

Kashiwagi, T., Yuasa, T., Tanabe, Y., Imai, T., Kuwano, G., Ota, R., Nakamura, K., Ono, Y., Kaneko, Y., Tsujimoto, M., Minami, H., Yamamoto, T., Klemm, R. A., & Kadowaki, K. (2018). Improved excitation mode selectivity of high- T_c superconducting terahertz emitters. *Journal of Applied Physics*, *124*(3), Article 033901. <https://doi.org/10.1063/1.5033914>

Important note

To cite this publication, please use the final published version (if applicable). Please check the document version above.

Copyright

Other than for strictly personal use, it is not permitted to download, forward or distribute the text or part of it, without the consent of the author(s) and/or copyright holder(s), unless the work is under an open content license such as Creative Commons.

Takedown policy

Please contact us and provide details if you believe this document breaches copyrights. We will remove access to the work immediately and investigate your claim.

Improved excitation mode selectivity of high- T_c superconducting terahertz emitters

Takanari Kashiwagi, Takumi Yuasa, Yuki Tanabe, Takayuki Imai, Genki Kuwano, Ryusei Ota, Kento Nakamura, Yukino Ono, Youta Kaneko, Manabu Tsujimoto, Hidetoshi Minami, Takashi Yamamoto, Richard A. Klemm, and Kazuo Kadowaki

Citation: *Journal of Applied Physics* **124**, 033901 (2018); doi: 10.1063/1.5033914

View online: <https://doi.org/10.1063/1.5033914>

View Table of Contents: <http://aip.scitation.org/toc/jap/124/3>

Published by the [American Institute of Physics](#)

Articles you may be interested in

[Circularly polarized terahertz radiation monolithically generated by cylindrical mesas of intrinsic Josephson junctions](#)

Applied Physics Letters **113**, 052601 (2018); 10.1063/1.5040159

[Thermoreflectance microscopy measurements of the Joule heating characteristics of high- \$T_c\$ superconducting terahertz emitters](#)

Journal of Applied Physics **122**, 233902 (2017); 10.1063/1.5002743

[Half-cycle terahertz surface waves with MV/cm field strengths generated on metal wires](#)

Applied Physics Letters **113**, 051101 (2018); 10.1063/1.5031873

[Intrinsic frequency tuning of terahertz quantum-cascade lasers](#)

Journal of Applied Physics **123**, 213102 (2018); 10.1063/1.5024480

[Perspective: Magnetoresistive sensors for biomedicine](#)

Journal of Applied Physics **124**, 030902 (2018); 10.1063/1.5027035

[Nonlinear thermal and electronic optical properties of graphene in N-methylpyrrolidone at 800 nm with femtosecond laser pulses](#)

Journal of Applied Physics **124**, 033104 (2018); 10.1063/1.5025781



Instruments for Advanced Science


Contact Hiden Analytical for further details:
W www.HidenAnalytical.com
E info@hiden.co.uk

CLICK TO VIEW our product catalogue



Gas Analysis

- dynamic measurement of reaction gas streams
- catalysis and thermal analysis
- molecular beam studies
- dissolved species probes
- fermentation, environmental and ecological studies



Surface Science

- UHV TPD
- SIMS
- end point detection in ion beam etch
- elemental imaging - surface mapping



Plasma Diagnostics

- plasma source characterization
- etch and deposition process reaction kinetic studies
- analysis of neutral and radical species



Vacuum Analysis

- partial pressure measurement and control of process gases
- reactive sputter process control
- vacuum diagnostics
- vacuum coating process monitoring

Improved excitation mode selectivity of high- T_c superconducting terahertz emitters

Takanari Kashiwagi,^{1,2} Takumi Yuasa,¹ Yuki Tanabe,¹ Takayuki Imai,¹ Genki Kuwano,¹ Ryusei Ota,¹ Kento Nakamura,¹ Yukino Ono,¹ Youta Kaneko,¹ Manabu Tsujimoto,^{1,2} Hidetoshi Minami,^{1,2} Takashi Yamamoto,³ Richard A. Klemm,⁴ and Kazuo Kadowaki^{1,2,5}

¹Graduate School of Pure and Applied Sciences, University of Tsukuba, 1-1-1 Tennodai, Tsukuba, Ibaraki 305-8573, Japan

²Division of Materials Science, Faculty of Pure and Applied Sciences, University of Tsukuba, 1-1-1, Tennodai, Tsukuba, Ibaraki 305-8573, Japan

³QuTech, Delft University of Technology, PO Box 5046, 2600 GA Delft, The Netherlands

⁴Department of Physics, University of Central Florida, 4111 Libra Drive, Orlando, Florida 32816-2385, USA

⁵Algae Biomass and Energy System R & D Center, University of Tsukuba, 1-1-1, Tennodai, Tsukuba, Ibaraki 305-8572, Japan

(Received 6 April 2018; accepted 26 June 2018; published online 16 July 2018)

Using our recent design of thermally managed sandwich device structures, we studied the radiation frequency characteristics of three such devices of the same rectangular dimensions made from the same single crystal of the high- T_c superconductor $\text{Bi}_2\text{Sr}_2\text{CaCu}_2\text{O}_{8+\delta}$, and all three devices exhibit similar characteristics. Their observed radiation intensities appear to be enhanced at many transverse magnetic $\text{TM}_{n,m}$ cavity mode frequencies, possibly including some higher $\text{TM}_{0,m}$ modes with waves solely along the rectangular length, none of which have previously been reported. In addition, the temperature dependences of the radiation frequencies correspond strongly to the temperature dependences of the maximum bias voltages applied to the devices. The excitations of many cavity modes higher in frequency than that of the usually observed $\text{TM}_{1,0}$ mode and the high reproducibility of the radiation frequency characteristics both appear to originate from the reduction in the Joule self-heating of the thermally managed sandwich structures. The information provided here should aid in the design of future devices to obtain the desired emission frequency ranges. Published by AIP Publishing. <https://doi.org/10.1063/1.5033914>

I. INTRODUCTION

In recent years, the development of high-performance terahertz (THz) emitters, detectors, and related devices have urgently been desired not only for purely scientific and technological reasons but also for their potential uses in many applications.^{1,2} Strong, coherent, and monochromatic THz electromagnetic (EM) waves are essential for modern communication technologies. Until recently, conventional semiconducting devices, such as resonant tunnel diodes^{3,4} and quantum cascade lasers,⁵⁻⁷ both of which employ modern nanotechnologies, have been widely considered to be the most promising methods to produce continuous and coherent sources in this frequency range. However, in 2007, the discoveries of strong, coherent, and continuous radiation obtained from one-dimensional stacks of intrinsic Josephson junctions (IJJs) in devices fabricated from single crystals of the high transition-temperature T_c superconductor $\text{Bi}_2\text{Sr}_2\text{CaCu}_2\text{O}_{8+\delta}$ (Bi2212) have provided a competitive field of research in this entire THz frequency range.⁸⁻¹³ In addition to spanning the entire frequency range from 0.3 to 11 THz,^{12,13} these superconducting IJJ-THz emitters have been shown to exhibit additional advantages over those leading semiconducting devices with regard to the coherent nature of the THz electromagnetic wave emission.

The IJJ-THz emitters based upon superconducting Bi2212 single crystals have intensively been developed both experimentally¹¹⁻⁶⁶ and theoretically.⁶⁷⁻⁸⁶ So far, the best

performance has been achieved within the frequency range from 0.3 to 11 THz,^{11-13,34,35,39} with the maximum output power of $\sim 30 \mu\text{W}$,^{31-34,39} and with a spectral width of the coherent and continuous emission of THz radiation that is generally less than 0.5 GHz, and under appropriate conditions, it was reported to be narrower than 23 MHz and possibly even 6 MHz.²³⁻²⁵ Furthermore, a synchronized operation of an array of three such emitters was reported to yield the greatly enhanced power of $610 \mu\text{W}$.²⁹ Most of the recent progress in developing these IJJ-THz emitters was reviewed and summarized.⁸⁷⁻⁸⁹

As for most micro-electronic devices, Joule heating in the IJJ-THz devices has been found to cause serious effects upon the device characteristics, especially with regard to the radiation frequency and intensity, and probably to its linewidth. The local temperature distributions $T(\mathbf{r})$ of the IJJ mesa devices have been measured in detail, and the results have been discussed in comparison with theoretical studies.^{14-16,40-45,51,63-66,78-80} These studies concluded that the spontaneous formation of a local temperature instability known as a hot spot can occur in the IJJ-THz emitter device due to both the quasi-two-dimensional thermal and electrical conductivities, the latter yielding a semiconducting-like temperature dependence of the c -axis normal state resistivity for under-doped Bi2212 single crystals. Previous studies revealed that a hot spot, within which the local temperature $T(\mathbf{r}) > T_c$, acts as a shunt resistance inserted parallel to the

N (of order 10^3) equivalent IJJs, which corresponds to the junction resistance in a resistively shunted junction (RSJ) model using an equivalent electrical circuit.

In the absence of a hot spot, the emission frequency f follows the ac Josephson relation, $f = 2ev/h$, where e and h are the electronic charge and Planck's constant, respectively, and $v = V/N$ is the applied voltage V per number N of active junctions. In this case, if all N_{tot} of the junctions in the stack are active in the emission process, and the maximum voltage that can be applied across the stack is V_m , the maximum emission frequency would be $f_j^m = (2e/h)V_m/N_{\text{tot}}$. The formation of the hot spot causes a reduction in the resultant voltage per active junction, reducing the maximum radiation frequency from that value. Moreover, experimental studies of hot spots have revealed that the position of the hot spot inside the device structure strongly affects the intensity but not the frequency of the IJJ-THz emissions.^{43–45} In addition, theoretical studies suggest that the inhomogeneous temperature distribution in the mesa could be the origin of the THz emission at the frequency of the most commonly observed transverse magnetic $\text{TM}_{1,0}$ EM cavity resonance of the mesa structure.^{71,82} These experimental and theoretical studies suggest that the hot spots must produce some effects on the THz emission characteristics.

Due to these characteristics mentioned earlier, it is evident that proper heat management to control the Joule self-heating, and, in particular, to limit the formation of the hot spot, is crucial in order to obtain high performance device characteristics. Recently, we proposed a device structure which efficiently reduces the Joule self-heating characteristics.^{12,39,54} The device is constructed from a stand-alone mesa (SAM) structure, with Au covering both the Bi2212 mesa's top and bottom, all of which is sandwiched between two metal-coated sapphire plates. Using this SAM structure of a disk-shaped Bi2212 device, we succeeded in increasing the radiation frequency range up to 2.4 THz, which was higher than in all previous devices.^{12,39,54} Very recently, however, this record was greatly broken with a much thinner and narrower rectangular Bi2212 device that was cut to produce two emitters and detectors, and emissions covering the entire 1–11 THz range were observed.¹³

Here, we show further progress obtained using our type of device structure. For most previous non-SAM rectangular devices, excitation of the $\text{TM}_{1,0}$ mode, consisting of a half

wavelength centered across the width of the device, was commonly observed.^{11,20,23} In such a device, we found a device which had excitation of the $\text{TM}_{2,0}$ mode, with a full wavelength across the width.²¹ Here, we applied our sandwich structure construction to three essentially identical rectangular SAMs, which have a slightly larger common width than those of rectangular SAMs studied previously. The present experimental results clearly show much wider ranges of radiation frequencies, with possible enhancements at many higher $\text{TM}_{n,m}$ cavity mode frequencies. We also compared the radiation characteristics of the three SAMs, and good reproducibility of the radiation frequency characteristics was obtained. The experimental results shown here should be helpful in the design of IJJ-THz emitters with strong emissions over desired frequency ranges.

II. SAMPLES AND EXPERIMENTAL SETUP

High-quality single crystals of Bi2212 were grown by a traveling-solvent floating-zone method using a modified infrared-image furnace.^{90,91} The Bi2212 single crystals were cleaved to obtain both fresh surfaces with a sample thickness on the order of a few micrometers. Both freshly cleaved surfaces were coated immediately with Ag and Au by evaporation in vacuum. The total thickness of the deposited metals is about 10 to 30 nm. Then, the stand-alone mesa structures were fabricated with an ion milling technique using metallic masks.¹⁹ Further details of the SAM fabrication procedure using the ion milling technique with metallic masks were reported previously.⁵⁴

A fabricated SAM is then sandwiched between two disk-shaped sapphire plates, as sketched in Fig. 1(b), onto which Au metal electrodes were deposited to produce good electrical contacts on the top and bottom surfaces of the SAM. The electrodes also provide good thermal contacts to the thermal bath. The diameter and thickness of the sapphire plates are 7.0 mm and 0.5 mm, respectively. The thicknesses and the widths of the deposited metals on the sapphire plates are 10 to 30 nm and 100 to 200 μm , respectively. The sapphire plates were clamped by four screws in a Cu-plate rig as sketched in the inset of Fig. 1(a). Finally, a hemispherical Si lens with 4 mm in diameter was attached to the front sapphire plate and held in place with a spacer.⁵⁴

The dimensions of the rectangular SAMs shown in Fig. 1(b) are $100 \times 410 \times 2.7 \mu\text{m}^3$, as estimated by an atomic

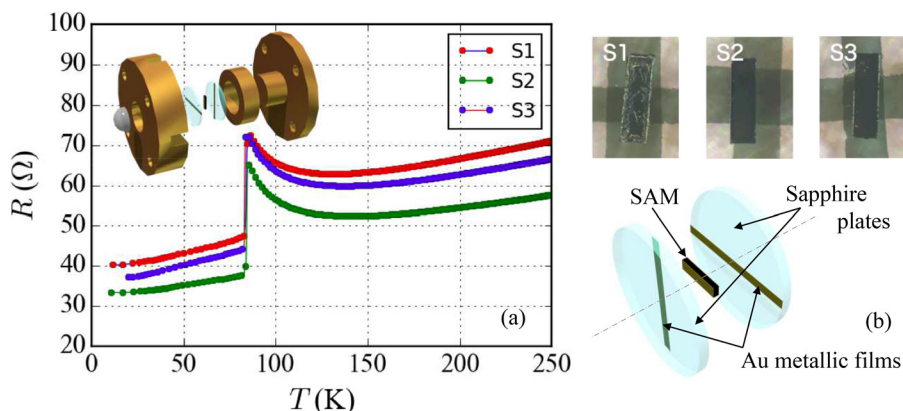


FIG. 1. (a) Plots of the temperature dependences of the c -axis resistances of the three samples denoted by S1, S2, and S3. The inset is a sketch of the assembled device structure. (b) Optical photographs of the three samples and a sketch of a SAM sandwich structure and its surroundings are shown.

force microscope and an optical microscope. From the thickness of $2.7\ \mu\text{m}$, the total number of Josephson junctions in each SAM can be estimated to be $N_{\text{tot}} \sim 1800$. The three samples denoted S1, S2, and S3 shown in Fig. 1(b) were prepared using this method. These SAMs were fabricated from the same piece of a Bi2212 single crystal. Due to a reassembly after the first assembly, the surface of sample S1 became slightly dirty.

For measurements of the radiation properties of the SAMs, we used a ^4He flow cryostat (CF1104, Oxford Instruments) for sample cooling, and a Si-bolometer (Infrared Laboratories) for detecting the emitted THz EM waves. To determine the radiation frequencies, a Fourier-transform infrared (FT-IR) spectrometer (FAIRS-1, JASCO) was used. It is noted that the FT-IR spectrometer contains three wire grids, and they were unchanged during the experiments. An FeRh thermometer was placed on the sample holder inside the ^4He flow cryostat to measure the bath temperature, T_b , of the sample. For measurements of the current-voltage characteristics (IVCs), a dc-voltage source and a standard resistor ($10\ \Omega$) were connected in series to supply both V and the corresponding dc-current, I , to the SAM structure. Further details of the experimental setup for measurements of the radiation properties were reported previously.^{20,23}

III. EXPERIMENTAL RESULTS

The main panel of Fig. 1 presents the temperature T dependence of the c -axis resistance of each of the three samples. At first glance, all three curves appear similar to within $\pm 20\%$. However, most of contribution to this variation appears to be a constant shift, perhaps originating from the different contact resistances used in the two-terminal measurements. Therefore, we estimate the resistances arising solely from the SAMs to be nearly the same to within $\pm 5\%$.

Figures 2(a) and 2(b) show the IVCs of the three SAMs (S1, S2, and S3) obtained at the respective bath temperatures $T_b = 30$ and 60 K. In these figures, the components of the additional resistances, such as those arising from the contacts

and from the gold thin films, have been subtracted from the data presented.

At $T_b = 30$ K, the three samples show large IVC hysteresis loops. The radiation at this temperature is mainly observed on the return branch of the IVCs in the so-called retrapping region, as shown in the bottom panel of Fig. 2(a). The hysteresis of the IVC loop shrinks with increasing bath temperature, as indicated in Fig. 2(b), the data for which were obtained at $T_b = 60$ K. Moreover, the radiation intensities are stronger around this bath temperature, as shown in the bottom panel of Fig. 2(b).

Some details of the temperature dependencies of the radiation intensity characteristics are discussed in the following. According to previous studies of the surface temperatures of mesa structures,^{42–45} hot spots appear to be correlated with the radiation characteristics and are significantly suppressed at higher bath temperatures. That is, the temperature gradient of the sample is smaller at higher bath temperatures. This effect of a more homogenous temperature distribution at higher rather than lower bath temperatures appears also to yield a large enhancement of the radiation intensity. Furthermore, the radiation intensity is also influenced by the resonances of the tunable ac-Josephson frequency with cavity mode frequencies appropriate for the SAM rectangular shape. We mainly discuss the radiation characteristics based upon those resonance conditions further in Secs. III and IV. However, further studies of the above factors are needed in order to understand our devices more precisely.

In order to evaluate the heat management characteristics of our sandwich structures, we estimated the SAM temperatures very roughly from previous studies of the T dependencies of the c -axis resistances and of the IVCs.^{11,41} The sample temperatures at $T_b = 30$ K are estimated from the IVC region of about 4–5 V at different bias currents to range from 40 to 60 K. For $T_b = 60$ K, the sample temperatures are estimated from the IVC region of about 2–3 V at different bias currents to be below 70 K. By using this sandwich structure, the heating of the sample temperature above T_b is

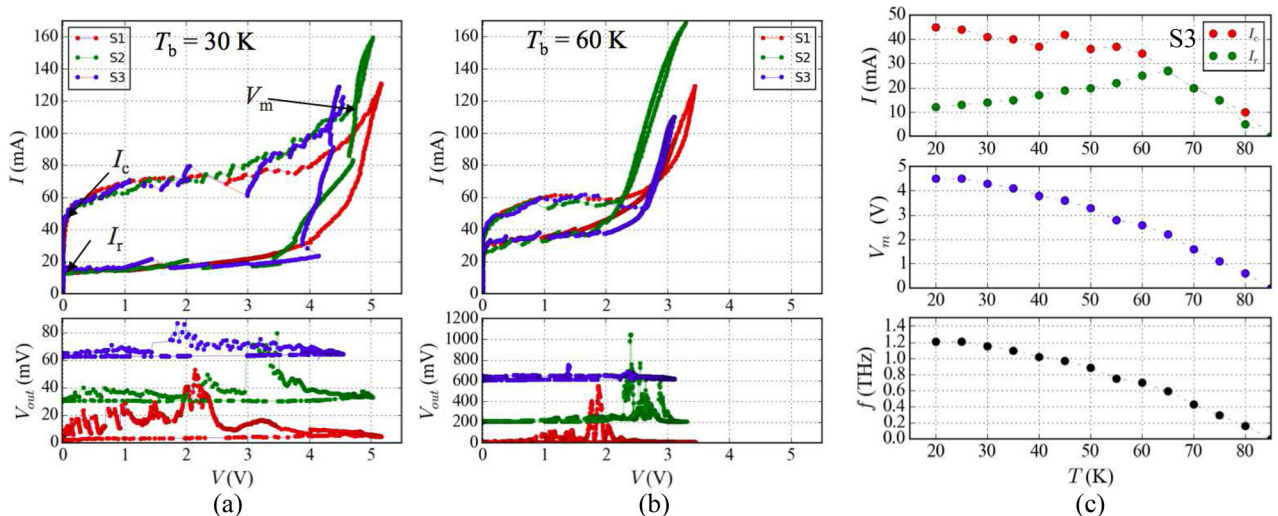


FIG. 2. The IVCs and the bias voltage dependences of the bolometer output voltages, V_{out} , of the three SAMs with the same dimensions of $100 \times 410 \times 2.7\ \mu\text{m}^3$ obtained at $T_b = 30$ K (a) and 60 K (b). (c) T_b dependences of I_c , I_r , V_m , and $f_J^m = (2e/h)V_m/N_{\text{tot}}$ for sample S3.

reduced from the heating of mesa structures fabricated on the surfaces of Bi2212 single crystals.

In general, the characteristic features of a Josephson junction are reflected in the critical current, I_c , the return current, I_r , and the maximum applied bias voltage, V_m , obtained from the IVCs. Note that the value of V_m is estimated from the maximum bias voltage of the closed hysteresis IVC loop obtained by sweeping the applied bias voltage up and down, as indicated by the arrow in Fig. 2(a). These characteristic values are estimated roughly from the temperature dependence of the IVCs and plotted in Fig. 2(c) for sample S3 as an example. The other two samples also showed similar behaviors. We also estimated the maximum radiation frequencies f_J^m from the value of V_m by using a modification of the ac Josephson relation expressed as $f_J^m = (2e/h)(V_m/N_{\text{tot}})$, which assumes the maximum applied voltage V_m is attained when all N_{tot} in each SAM are active in the emissions. The observed temperature dependence of the radiation frequency characteristics is well explained by f_J^m , as discussed further in Sec. III.

Figure 3 shows the bath temperature dependence of the radiation spectrum observed from the three samples. The spectra displayed from top to bottom correspond to increasing bath temperature. As explained in Fig. 2, the radiation was mainly observed on the return branch region of the IVCs. In this current-voltage region, it is well known that the number of working Josephson junctions changes in increments corresponding to small jumps in the applied bias voltage. This kind of behavior could result in some amount of decoherence of the working intrinsic Josephson junctions in the mesa structure. Such decoherence is indeed seen in the multiple radiation peaks at the foot of the major radiation peak, as observed in the lower temperature spectra at 20, 30, and 50 K in Fig. 3. At higher temperatures, the radiation

spectrum (55–65 K) at the 2nd harmonic frequency denoted by the black arrows is seen, but it is known to be a ghost signal arising from the spectrometer characteristics.¹²

The largest peak in each of the radiation frequency spectra observed from the three samples shifts from higher to lower frequency as the bath temperature is increased. Moreover, the spectral peak intensities appear to be enhanced over a particular temperature region. This behavior is observed in a wide frequency range. These temperature-dependent intensities and frequencies are consistent with the frequency matching between a cavity resonance frequency determined by the shape and the size of the SAM structure and the ac Josephson effect determined by the applied bias voltage to the IJJs. It is also noted here that all of these features are consistent with the results observed in previous studies.^{20,23}

The relationships between the observed radiation frequencies and their spectral peak intensities are displayed in Fig. 4(a) for the three samples. The symbol color corresponds to the bath temperature in the corresponding far right bar code. It is clear that the radiation frequency characteristics are very similar for the three samples. As noted above, higher radiation frequencies are observed at lower bath temperatures. The radiation frequency shifts to lower values as the bath temperature increases. These characteristics can be seen very well in Fig. 4(a). In addition, the radiation intensities show clear peaks at around 0.7 and 1.1 THz, but large intensities are observed at many frequencies. These overall enhancements of the radiation intensity can be explained by considering the excitations of many EM cavity modes, as discussed in the following.

From the data shown in Fig. 4(a), we plotted the relationship between the radiation frequencies and the bath temperatures in Fig. 4(b). In this figure, the color and size of the

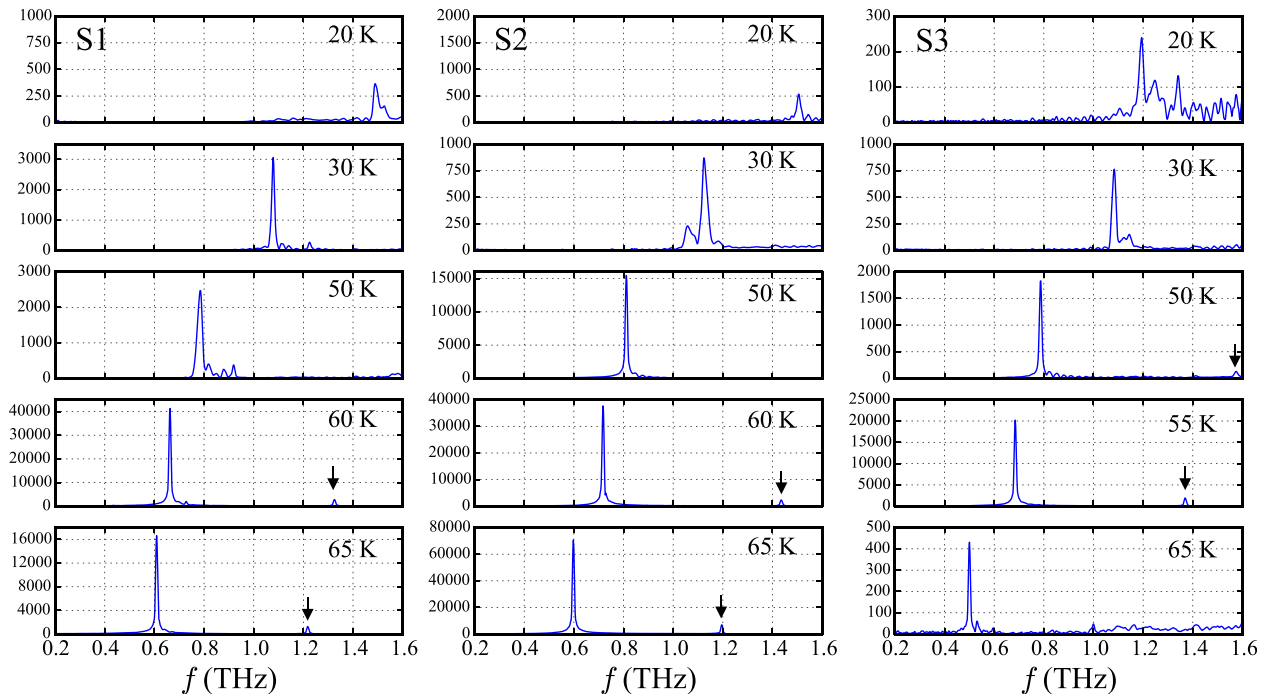


FIG. 3. The radiation spectral intensity in counts versus f for the three samples at the indicated T_b values. The black arrows indicate the ghost signals attributed to the fundamental frequency.

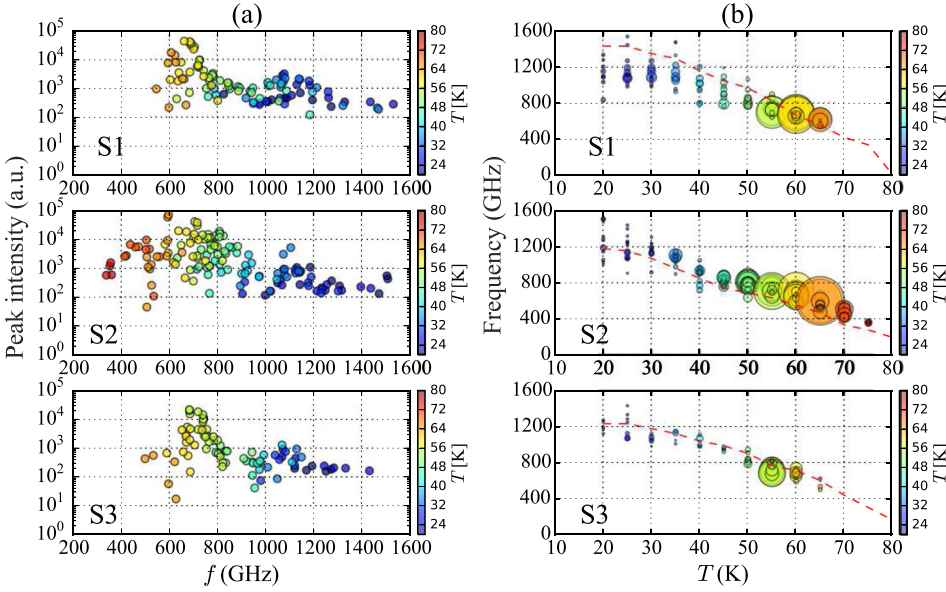


FIG. 4. (a) Logarithmic plots of the spectral peak intensity versus radiation frequency as measured by the FT-IR spectrometer for the three samples. The symbol colors correspond to the bath temperatures in the far right bar codes. (b) Plots of the radiation frequency versus the bath temperature obtained from the same data presented in Fig. 4(a). The red dashed curves represent the radiation frequencies estimated from f_j^m as shown for sample S3 in the bottom panel of Fig. 2(c).

symbol indicate the bath temperature and the spectrum peak intensity, respectively. From this data plot, both the frequency and the intensity of the radiation can be easily seen to be a strong function of T_b . The hysteresis of the IVC loop shrinks with increasing bath temperature. Therefore, as shown in the middle panel of Fig. 2(c), V_m also decreases with increasing T_b . According to our modified Josephson relation $f_j^m = (2e/h)(V_m/N_{\text{tot}})$, the maximum radiation frequency, f_j^m , also decreases with increasing T_b . The observed temperature dependence of the radiation frequency is well explained by the estimated radiation frequency f_j^m from V_m presented in the caption in Fig. 2(c), and this relationship is displayed by the red dashed curves in Fig. 4(b).

We replotted the relationship between the observed radiation frequency and the applied bias voltage in Fig. 5 using the same data shown in Fig. 4. The colors correspond to T_b in the bar codes, and the sizes of the symbols correspond to

the spectral peak intensities. The blue dashed lines indicate the ac-Josephson relation estimated from the thickness of the mesa structure corresponding to $N_{\text{tot}} \sim 1800$ Josephson junctions. The horizontal red dashed lines indicate the regions corresponding to different transverse magnetic patch antenna mode ranges denoted by the lowest $\text{TM}_{n,0}$ mode frequencies for each $\text{TM}_{n,m}$ mode series with n half-wavelengths across the mesa widths. Snapshot images of the electric field distribution in the xy -plane oscillating along the z -direction calculated using patch antenna theory are plotted in Fig. 5 just below those red dashed lines.

The data plotted on the frequency-voltage plane of Fig. 5 clearly indicate the connection between the radiation frequency and the ac-Josephson relation. Note that the deviations between the blue dashed lines and the observed data points are attributed to the fact that the number N of working junctions in the retrapping IVC region is smaller than N_{tot} .

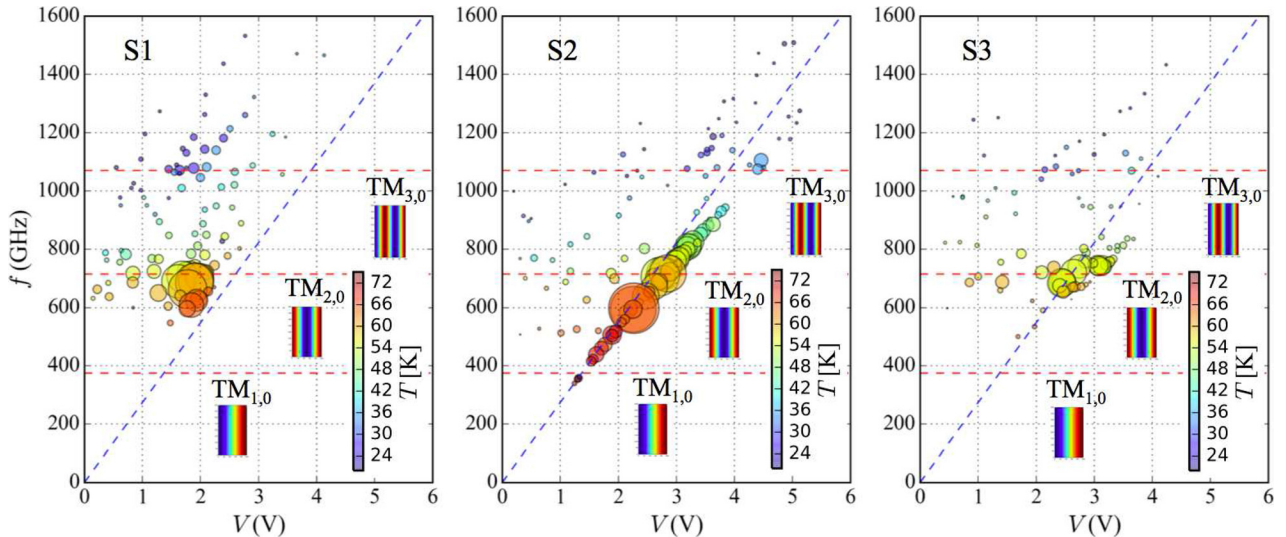


FIG. 5. Plots of the radiation frequency versus the applied bias voltage for the data obtained from the three mesa structures. The blue dashed lines indicate the ac Josephson relation $f_j = (2e/h)V/N$, where N is assumed to be N_{tot} , as estimated from the thickness of the SAMs. The red dashed lines indicate the cavity mode frequencies $f_{n,0}^c$ for $n = 1$ to 3 from Eq. (2), as estimated from the common width w of the SAMs. Snapshot images of the corresponding two-dimensional distributions of the E_z component of those three cavity mode waves are also displayed near the red lines.

The three samples show similar behaviors in this frequency-voltage plane. The radiation intensities are clearly enhanced at the $\text{TM}_{2,0}$ mode frequency of ~ 0.7 THz, but are either weak or not observed at the commonly observed $\text{TM}_{1,0}$ mode frequency of ~ 0.36 THz. In addition, the radiation intensities are slightly enhanced at around the $\text{TM}_{3,0}$ mode frequency of ~ 1.1 THz. However, all three samples indicate radiation at many additional frequencies. In order to confirm those mode identifications, we need to obtain information regarding the radiation distribution by measuring the angular dependence of the emission intensity and polarization in more detail.

We further note that the radiation from sample S2 is the strongest at around 0.6 THz, which deviates slightly from the calculated $\text{TM}_{2,0}$ mode frequency. Although we tried to measure the radiation spectrum as many different IVC bias points as possible, it was experimentally difficult to measure the radiation spectra at all bias voltage points and bath temperatures. In addition, it is still not clear how strongly the structures such as the thin gold films and sapphire substrates surrounding the SAMs contribute to the observed output frequencies. These structures should contribute to the cavity resonance frequencies. Future studies are needed to clarify the details of these effects.

IV. THEORETICAL CONSIDERATIONS

Nevertheless, it is possible to further analyze the possible cavity mode excitations by including the full symmetry of the rectangular point group C_{2v} . For a thin rectangular device structure of width w and length ℓ , the normalized TM wave functions $\Psi_{n,m}(x, y)$ for the magnetic vector potential A_z (and the electric field E_z) of the cavity modes satisfying the Neumann boundary conditions (with vanishing normal derivatives on each of the boundaries^{85,86}) may be written as

$$\Psi_{n,m}(x, y) = \frac{2}{\sqrt{w\ell}} \cos(n\pi x/w) \cos(m\pi y/\ell), \quad (1)$$

where for simplicity we take the lower left and upper right corners of the rectangle to be, respectively, at the origin and at the point (w, ℓ) . For a rectangular microstrip antenna, all of the $\text{TM}_{n,m}$ modes are one-dimensional representations of the C_{2v} point group,⁸⁶ and therefore have fixed nodal line positions during the amplification process of a resonance.^{76,85,86} The frequencies $f_{n,m}^c$ of the resonant cavity modes are then easily found to be⁸⁶

$$f_{n,m}^c = \frac{c_0}{2n_r} \sqrt{(n/w)^2 + (m/\ell)^2}, \quad (2)$$

where c_0 is the speed of light in vacuum and $n_r \approx 4.2$ is the index of refraction for samples with thicknesses on the order of $1 \mu\text{m}$ or greater, as found previously. In past experiments, no emission was observed for $f \leq f_{pl} \approx 0.3$ THz, the Josephson plasma frequency for Bi2212 samples at least $1 \mu\text{m}$ thick. The calculated resonance frequencies for all modes in the observed range $0.35 < f < 1.6$ THz are listed in Table I. To distinguish small differences between some mode frequencies, we set $n_r = 4.20$ in this table. Note that

TABLE I. Calculated transverse magnetic cavity mode frequencies $f_{n,m}^c$ in THz in the observed range $0.35 \text{ THz} \leq f_{n,m}^c < 1.6 \text{ THz}$ for a thin rectangular device with $w = 100 \mu\text{m}$, $\ell = 410 \mu\text{m}$, and $n_r = 4.20$.

m	$f_{0,m}^c$	$f_{1,m}^c$	$f_{2,m}^c$	$f_{3,m}^c$	$f_{4,m}^c$
0		0.357	0.714	1.07	1.43
1		0.367	0.719	1.08	1.43
2		0.397	0.735	1.09	1.44
3		0.442	0.760	1.10	1.45
4	0.348	0.499	0.794	1.13	1.47
5	0.436	0.563	0.836	1.16	1.49
6	0.523	0.633	0.885	1.19	1.52
7	0.610	0.706	0.939	1.23	1.55
8	0.697	0.782	0.998	1.28	1.59
9	0.784	0.861	1.06	1.33	
10	0.871	0.941	1.13	1.38	
11	0.958	1.02	1.20	1.44	
12	1.05	1.10	1.27	1.50	
13	1.13	1.19	1.34	1.56	
14	1.22	1.27	1.41		
15	1.31	1.35	1.49		
16	1.39	1.44	1.56		
17	1.48	1.52			
18	1.57				

according to our previous studies, the excitation modes along the width of the rectangular mesa structure, i.e., the $\text{TM}_{n,0}$ modes, are commonly observed for rectangular mesa structures. However, excitations of $\text{TM}_{n,m}$ modes with $m \neq 0$ appear also to be active in the present studies, and modes with $n = 0$ with $4 \leq m \leq 18$ also lie in this range, and cannot be excluded from consideration in the absence of angular distribution and polarization studies.

In Figs. 6–8, we present contour plots of snapshot images of some representative electric field wave functions of the $\text{TM}_{n,m}$ modes present in Table I. In each of these figures, the red and blue regions correspond, respectively, to the most positive and negative snapshot values, and the thick black lines are fixed wave function nodes. For a general $\text{TM}_{n,m}$ mode, the wave function given by Eq. (1) has n nodes across the width and m nodes along the length. In Fig. 6,

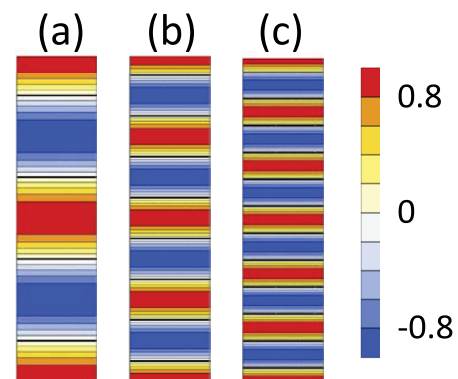


FIG. 6. Contour plot snapshot images of the two-dimensional distributions of the E_z component of three representative $\text{TM}_{0,m}$ cavity modes with $m = 4, 8, 12$. The darkest red and blue regions are the most positive and negative in value, and the thick black lines are nodes. The color code is in units of $1/w$ with $\ell = 4.1w$ and adjacent colors differ by $0.2/w$. (a) $\text{TM}_{0,4}$, (b) $\text{TM}_{0,8}$, and (c) $\text{TM}_{0,12}$.

three observable (*i.e.*, exceeding f_{pl}) $TM_{0,m}$ mode wave functions with $m = 4, 8,$ and 12 are pictured. In Fig. 7, four representative $TM_{1,m}$ modes with $m = 0, 1, 2,$ and 5 are shown. We note that the predicted $TM_{0,4}$ mode at 0.348 THz pictured in Fig. 6(a) is nearly degenerate with the usually observed $TM_{1,0}$ mode (at 0.357 THz) pictured in Fig. 7(a) for this particular w/ℓ ratio. Either or both of these modes and/or possibly the $TM_{1,1}$ mode at 0.367 THz pictured in Fig. 7(b) may correspond to the two points lying below the lowest horizontal red dashed line of the data observed from sample S2 pictured in Fig. 5. They might be distinguishable by comparisons of detailed angular distribution studies of the radiation with calculated predictions, as was done previously.⁷⁹ However, precise mode wave function determination from such comparisons can be difficult to make unless the intensities from the cavity mode emissions greatly exceeds that from the uniform Josephson current source.^{75,76,79} We further note that the very strong emission from sample S2 near to 0.60 THz could correspond to either the $TM_{0,7}$ or $TM_{1,6}$ modes that are predicted from Eq. (2) to emit at 0.610 and 0.633 THz, respectively. Such modes also appear to be prominent outputs from sample S1, as seen in the left panel to Fig. 5. Possible evidence for the excitations of the $TM_{0,8}$ and $TM_{1,7}$ modes at 0.696 and 0.706 THz, respectively, is present in the data obtained from all three samples. A snapshot image of the $TM_{0,8}$ mode is pictured in Fig. 6(b). We note that if these tentative assignments are correct, some of the data presented in Fig. 5 would be the first evidence of emissions from waves solely along the length of rectangular Bi2212 devices.

In Fig. 8, the four representative $TM_{2,m}$ wave functions with $m = 0, 1, 2,$ and 5 are shown. We note that sample S2 appears to show considerable emissions from either the $TM_{2,m}$ modes with $m = 0$ to 7 or the $TM_{1,m}$ modes with $m = 7$ to 10 . All three samples show some emissions from the $TM_{3,m}$ modes with $m = 0$ to 13 , and possibly from the $TM_{4,m}$ modes with $m = 0$ to 8 . But such emissions are relatively weak.

This enhancement of the higher cavity mode excitations for $T_b \sim 60$ K is attributed to the significant reduction in the

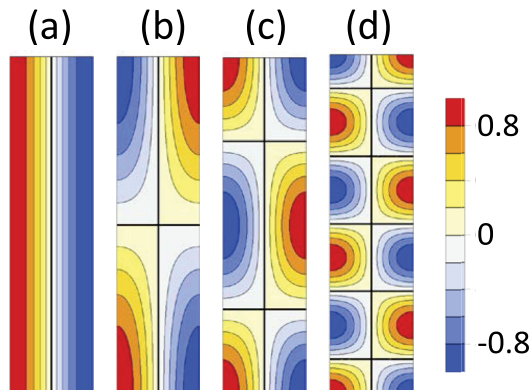


FIG. 7. Contour plot snapshot images of the two-dimensional distributions of the E_z component of four representative $TM_{1,m}$ cavity modes with $m = 0, 1, 2,$ and 5 . The darkest red and blue regions are the most positive and negative in value, and the thick black lines are nodes. The color code is in units of $1/w$ with $\ell = 4.1w$ and adjacent colors differ by $0.2/w$. (a) $TM_{1,0}$, (b) $TM_{1,1}$, (c) $TM_{1,2}$, and (d) $TM_{1,5}$.

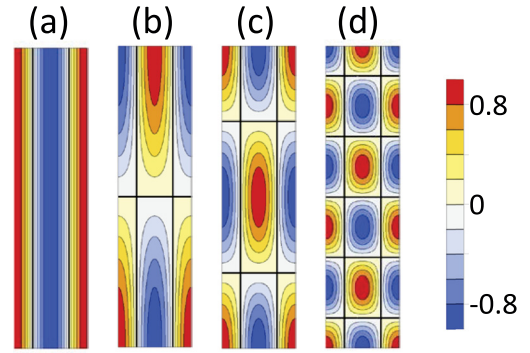


FIG. 8. Snapshot images of the two-dimensional distributions of the E_z component of four representative $TM_{2,m}$ cavity modes with $m = 0, 1, 2,$ and 5 . The darkest red and blue regions are the most positive and negative in value, and the thick black lines are nodes. The color code is in units of $1/w$ with $\ell = 4.1w$ and adjacent colors differ by $0.2/w$. (a) $TM_{2,0}$, (b) $TM_{2,1}$, (c) $TM_{2,2}$, and (d) $TM_{2,5}$.

Joule self-heating of the mesa devices due to their overall sandwich structure. We compared the data obtained from the three samples at the same bath temperature. For these samples, higher bias voltages can be applied to the mesa devices than were possible with previous conventional device structures supported by superconducting Bi2212 substrates. The new data suggest that the $V_m - T_b$ curve is determined by the dimensions of the mesa structures, the doping level of the Bi2212 single crystals, the cooling power of the measurement system, and the heat reduction capability of the device structures. This $V_m - T_b$ relationship is very important in order to obtain strong enhancement of the radiation intensity at particular cavity mode frequencies. According to the experimental results presented here, it is possible to obtain the strongest radiation with a desired frequency by adjusting V_m to match a particular $TM_{m,n}$ mode depending on the shape and size of the mesa. This allows one to select the excitation modes with the desired frequency ranges and to design high-powered IJJ-THz emitters.

V. CONCLUSIONS

In conclusion, we have studied the radiation frequency characteristics of three rectangular mesa structures with the same dimensions of $100 \times 410 \times 2.7 \mu\text{m}^3$, each fabricated from the same piece of a single crystal of the high- T_c superconductor $\text{Bi}_2\text{Sr}_2\text{CaCu}_2\text{O}_{8+\delta}$. The observed radiation intensities appear to be enhanced at the $TM_{n,m}$ modes considerably higher in frequency than the $TM_{1,0}$ mode seen in most previous emissions from rectangular samples of that material. Not only are emissions corresponding to the $TM_{2,0}$ and $TM_{3,0}$ modes probably observed, emissions at the $TM_{1,m}$, $TM_{2,m}$ and $TM_{3,m}$ modes appear to have been observed for high m values, and possible emissions of the $TM_{0,m}$ modes for $m \geq 4$ up to at least 8 or higher may also have been observed. If true, this would be the first report of the excitations of cavity modes with the waves along the lengths of the rectangular devices. The emission characteristics of the three samples are very similar. In addition, the observed temperature dependence of the radiation frequencies are well explained by the maximum applied bias voltage to the mesa devices.

The excitation of higher cavity modes and the good reproducibility of the radiation characteristics are thought to originate from the reduction of the Joule self-heating of the mesa devices obtained from the device sandwich structure described here. The information obtained in the present study should prove helpful and important for the development of well-characterized THz emitters with higher power at the desired frequency ranges.

ACKNOWLEDGMENTS

This work was supported by JSPS KAKENHI Grant No. JP15H01996. T.K. was also supported by JSPS KAKENHI Grant No. JP17K05018.

- ¹B. Ferguson and X. C. Zhang, *Nat. Mater.* **1**, 26 (2002).
- ²M. Tonouchi, *Nat. Photonics* **1**, 97 (2007).
- ³Y. Koyama, R. Sekiguchi, and T. Ouchi, *APEX* **6**, 064102 (2013).
- ⁴H. Kanaya, R. Sogabe, T. Maekawa, S. Suzuki, and M. Asada, *J. Infrared Millimeters, Terahertz Waves* **35**, 425 (2014).
- ⁵C. Walthers, M. Fischer, G. Scalari, R. Terazzi, N. Hoyler, and J. Faist, *Appl. Phys. Lett.* **91**, 131122 (2007).
- ⁶S. Fatholouloumi, E. Dupont, C. W. I. Chan, Z. R. Wasilewski, S. R. Laframboise, D. Ban, A. Mátyás, C. Jirauschek, Q. Hu, and H. C. Liu, *Opt. Express* **20**, 3866 (2012).
- ⁷J. Kiessling, I. Breunig, P. G. Schunemann, K. Buse, and K. Vodopyanov, *New J. Phys.* **15**, 105014 (2013).
- ⁸R. Kleiner, F. Steinmeyer, G. Kunkel, and P. Müller, *Phys. Rev. Lett.* **68**, 2394 (1992).
- ⁹R. Kleiner and P. Müller, *Phys. Rev. B* **49**, 1327 (1994).
- ¹⁰A. A. Yurgens, *Supercond. Sci. Technol.* **13**, R85 (2000).
- ¹¹L. Ozyuzer, A. E. Koshelev, C. Kurter, N. Gopalsami, Q. Li, M. Tachiki, K. Kadowaki, T. Yamamoto, H. Minami, H. Yamaguchi *et al.*, *Science* **318**, 1291 (2007).
- ¹²T. Kashiwagi, K. Sakamoto, H. Kubo, Y. Shibano, T. Enomoto, T. Kitamura, K. Asanuma, T. Yasui, C. Watanabe, K. Nakade *et al.*, *Appl. Phys. Lett.* **107**, 082601 (2015).
- ¹³E. A. Borodiansky and V. M. Krasnov, *Nat. Commun.* **8**, 1742 (2017).
- ¹⁴H. B. Wang, S. Guénon, J. Yuan, A. Iishi, S. Arisawa, T. Hatano, T. Yamashita, D. Koelle, and R. Kleiner, *Phys. Rev. Lett.* **102**, 017006 (2009).
- ¹⁵H. B. Wang, S. Guénon, B. Gross, J. Yuan, Z. G. Jiang, Y. Y. Zhong, M. Grünzweig, A. Iishi, P. H. Wu, T. Hatano, D. Koelle, and R. Kleiner, *Phys. Rev. Lett.* **105**, 057002 (2010).
- ¹⁶S. Guénon, M. Grünzweig, B. Gross, J. Yuan, Z. G. Jiang, Y. Y. Zhong, M. Y. Li, A. Iishi, P. H. Wu, T. Hatano *et al.*, *Phys. Rev. B* **82**, 214506 (2010).
- ¹⁷T. M. Benseman, A. E. Koshelev, K. E. Gray, W.-K. Kwok, U. Welp, K. Kadowaki, M. Tachiki, and T. Yamamoto, *Phys. Rev. B* **84**, 064523 (2011).
- ¹⁸H. Koseoglu, F. Turkoglu, Y. Simsek, and L. Ozyuzer, *J. Supercond. Nov. Magn.* **24**, 1083 (2011).
- ¹⁹H. Minami, I. Takeya, H. Yamaguchi, T. Yamamoto, and K. Kadowaki, *Appl. Phys. Lett.* **95**, 232511 (2009).
- ²⁰K. Kadowaki, M. Tsujimoto, K. Yamaki, T. Yamamoto, T. Kashiwagi, H. Minami, M. Tachiki, and R. A. Klemm, *J. Phys. Soc. Jpn.* **79**, 023703 (2010).
- ²¹T. Kashiwagi, K. Yamaki, M. Tsujimoto, K. Deguchi, N. Orita, T. Koike, R. Nakayama, H. Minami, T. Yamamoto, R. A. Klemm, M. Tachiki, and K. Kadowaki, *J. Phys. Soc. Jpn.* **80**, 094709 (2011).
- ²²M. Tsujimoto, T. Yamamoto, K. Delfanazari, R. Nakayama, T. Kitamura, M. Sawamura, T. Kashiwagi, H. Minami, M. Tachiki, K. Kadowaki, and R. A. Klemm, *Phys. Rev. Lett.* **108**, 107006 (2012).
- ²³T. Kashiwagi, M. Tsujimoto, T. Yamamoto, H. Minami, K. Yamaki, K. Delfanazari, K. Deguchi, N. Orita, T. Koike, R. Nakayama *et al.*, *Jpn. J. Appl. Phys.* **51**, 010113 (2012).
- ²⁴M. Li, J. Yuan, N. Kinev, J. Li, B. Gross, S. Guénon, A. Ishii, K. Hirata, T. Hatano, D. Koelle *et al.*, *Phys. Rev. B* **86**, 060505 (2012).
- ²⁵H. B. Wang, M. Y. Li, J. Yuan, N. Kinev, J. Li, B. Gross, S. Guénon, A. Ishii, T. Hatano, D. Koelle *et al.*, *IEEE Proceedings of 37th International Conference on Infrared, Millimeter, and Terahertz Waves* (2012).
- ²⁶H. Minami, M. Tsujimoto, T. Kashiwagi, T. Yamamoto, and K. Kadowaki, *IEICE Trans. Electron.* **E95-C**, 347 (2012).
- ²⁷I. Takeya, Y. Omukai, T. Yamamoto, K. Kadowaki, and M. Suzuki, *Appl. Phys. Lett.* **100**, 242603 (2012).
- ²⁸F. Turkoglu, H. Koseoglu, Y. Demirhan, L. Ozyuzer, S. Preu, S. Malzer, Y. Simsek, P. Müller, T. Yamamoto, and K. Kadowaki, *Supercond. Sci. Technol.* **25**, 125004 (2012).
- ²⁹T. M. Benseman, K. E. Gray, A. E. Koshelev, W.-K. Kwok, U. Welp, H. Minami, K. Kadowaki, and T. Yamamoto, *Appl. Phys. Lett.* **103**, 022602 (2013).
- ³⁰J. Yuan, M. Y. Li, J. Li, B. Gross, A. Ishii, K. Yamaura, T. Hatano, K. Hirata, E. Takayama-Muromachi, P. H. Wu *et al.*, *Supercond. Sci. Technol.* **25**, 075015 (2012).
- ³¹D. Y. An, J. Yuan, N. Kinev, M. Y. Li, Y. Huang, M. Ji, H. Zhang, Z. L. Sun, L. Kang, B. B. Jin *et al.*, *Appl. Phys. Lett.* **102**, 092601 (2013).
- ³²S. Sekimoto, C. Watanabe, H. Minami, T. Yamamoto, T. Kashiwagi, R. A. Klemm, and K. Kadowaki, *Appl. Phys. Lett.* **103**, 182601 (2013).
- ³³K. Kadowaki, M. Tsujimoto, K. Delfanazari, T. Kitamura, M. Sawamura, H. Asai, T. Yamamoto, K. Ishida, C. Watanabe, S. Sekimoto *et al.*, *Physica C* **491**, 2 (2013).
- ³⁴T. Kitamura, T. Kashiwagi, T. Yamamoto, M. Tsujimoto, C. Watanabe, K. Ishida, S. Sekimoto, K. Asanuma, T. Yasui, K. Nakade *et al.*, *Appl. Phys. Lett.* **105**, 202603 (2014).
- ³⁵M. Ji, J. Yuan, B. Gross, F. Rudau, D. Y. An, M. Y. Li, X. J. Zhou, Y. Huang, H. C. Sun, Q. Zhu *et al.*, *Appl. Phys. Lett.* **105**, 122602 (2014).
- ³⁶K. Delfanazari, H. Asai, M. Tsujimoto, T. Kashiwagi, T. Kitamura, T. Yamamoto, M. Sawamura, K. Ishida, C. Watanabe, S. Sekimoto *et al.*, *Opt. Express* **21**, 2171–2184 (2013).
- ³⁷K. Delfanazari, H. Asai, M. Tsujimoto, T. Kashiwagi, T. Kitamura, T. Yamamoto, M. Sawamura, K. Ishida, M. Tachida, R. A. Klemm, T. Hattori, and K. Kadowaki, *Physica C* **491**, 16 (2013).
- ³⁸K. Delfanazari, H. Asai, M. Tsujimoto, T. Kashiwagi, T. Kitamura, T. Yamamoto, W. Wilson, R. A. Klemm, T. Hattori, and K. Kadowaki, *IEEE Trans. Terahertz Sci. Technol.* **5**, 505 (2015).
- ³⁹T. Kashiwagi, T. Yamamoto, T. Kitamura, K. Asanuma, C. Watanabe, K. Nakade, T. Yasui, Y. Saiwai, Y. Shibano, H. Kubo *et al.*, *Appl. Phys. Lett.* **106**, 092601 (2015).
- ⁴⁰S. Niratisairak, Ø. Haugen, T. H. Johansen, and T. Ishibashi, *Physica C* **468**, 442 (2008).
- ⁴¹T. M. Benseman, A. E. Koshelev, W.-K. Kwok, U. Welp, V. K. Vlasko-Vlasov, K. Kadowaki, H. Minami, and C. Watanabe, *J. Appl. Phys.* **113**, 133902 (2013).
- ⁴²H. Minami, C. Watanabe, K. Sato, S. Sekimoto, T. Yamamoto, T. Kashiwagi, R. A. Klemm, and K. Kadowaki, *Phys. Rev. B* **89**, 054503 (2014).
- ⁴³C. Watanabe, H. Minami, S. Sekimoto, T. Yamamoto, T. Kashiwagi, R. A. Klemm, and K. Kadowaki, *J. Phys.: Condens. Matter* **26**, 172201 (2014).
- ⁴⁴M. Tsujimoto, H. Kambara, Y. Maeda, Y. Yoshioka, Y. Nakagawa, and I. Takeya, *Phys. Rev. Appl.* **2**, 044016 (2014).
- ⁴⁵C. Watanabe, H. Minami, T. Kitamura, K. Asanuma, K. Nakade, T. Yasui, Y. Saiwai, Y. Shibano, T. Yamamoto, T. Kashiwagi, R. A. Klemm, and K. Kadowaki, *Appl. Phys. Lett.* **106**, 042603 (2015).
- ⁴⁶M. Tsujimoto, K. Yamaki, K. Deguchi, T. Yamamoto, T. Kashiwagi, H. Minami, M. Tachiki, K. Kadowaki, and R. A. Klemm, *Phys. Rev. Lett.* **105**, 037005 (2010).
- ⁴⁷M. Tsujimoto, H. Minami, K. Delfanazari, M. Sawamura, R. Nakayama, T. Kitamura, T. Yamamoto, T. Kashiwagi, T. Hattori, and K. Kadowaki, *J. Appl. Phys.* **111**, 123111 (2012).
- ⁴⁸T. Kashiwagi, K. Nakade, B. Markovic, Y. Saiwai, H. Minami, T. Kitamura, C. Watanabe, K. Ishida, S. Sekimoto, K. Asanuma *et al.*, *Appl. Phys. Lett.* **104**, 022601 (2014).
- ⁴⁹T. Kashiwagi, K. Nakade, Y. Saiwai, H. Minami, T. Kitamura, C. Watanabe, K. Ishida, S. Sekimoto, K. Asanuma, T. Yasui *et al.*, *Appl. Phys. Lett.* **104**, 082603 (2014).
- ⁵⁰Y. Demirhan, H. Saglam, F. Turkoglu, H. Alaboz, L. Ozyuzer, N. Miyakawa, and K. Kadowaki, *Vacuum* **120**, 89 (2015).
- ⁵¹F. Rudau, M. Tsujimoto, B. Gross, T. E. Judd, R. Wieland, E. Goldobin, N. Kinev, J. Yuan, Y. Huang, M. Ji *et al.*, *Phys. Rev. B* **91**, 104513 (2015).
- ⁵²F. Rudau, R. Wieland, J. Langer, X. J. Zhou, M. Ji, N. Kinev, L. Y. Hao, Y. Huang, J. Li, P. H. Wu *et al.*, *Phys. Rev. Appl.* **5**, 044017 (2016).
- ⁵³M. Tsujimoto, Y. Maeda, H. Kambara, A. Elarabi, Y. Yoshioka, Y. Nakagawa, Y. Wen, T. Doi, H. Saito, and I. Takeya, *Supercond. Sci. Technol.* **28**, 105015 (2015).

- ⁵⁴T. Kashiwagi, T. Yamamoto, H. Minami, M. Tsujimoto, R. Yoshizaki, K. Delfanazari, T. Kitamura, C. Watanabe, K. Nakade, T. Yasui *et al.*, *Phys. Rev. Appl.* **4**, 054018 (2015).
- ⁵⁵H. Minami, C. Watanabe, T. Kashiwagi, T. Yamamoto, K. Kadowaki, and R. A. Klemm, *J. Phys.: Condens. Matter* **28**, 025701 (2016).
- ⁵⁶M. Tsujimoto, I. Takeya, T. Kashiwagi, H. Minami, and K. Kadowaki, *Opt. Express* **24**, 4591 (2016).
- ⁵⁷L. Y. Hao, M. Ji, J. Yuan, D. Y. An, M. Y. Li, X. J. Zhou, Y. Huang, H. C. Sun, Q. Zhu, F. Rudau *et al.*, *Phys. Rev. Appl.* **3**, 024006 (2015).
- ⁵⁸L. Y. Hao, X. J. Zhou, Z. B. Yang, H. L. Zhang, H. C. Sun, H. X. Cao, P. H. Dai, J. Li, T. Hatano, H. B. Wang, Q. Y. Wen, and P. H. Wu, *Appl. Phys. Lett.* **109**, 233503 (2016).
- ⁵⁹K. Nakade, T. Kashiwagi, Y. Saiwai, H. Minami, T. Yamamoto, R. A. Klemm, and K. Kadowaki, *Sci. Rep.* **6**, 23178 (2016).
- ⁶⁰O. Kizilaslan, F. Rudau, R. Wieland, J. S. Hampp, X. J. Zhou, M. Ji, O. Kiselev, N. Kinev, Y. Huang, L. Y. Hao *et al.*, *Supercond. Sci. Technol.* **30**, 034006 (2017).
- ⁶¹H. Sun, Z. Yang, N. V. Kinev, O. S. Kiselev, Y. Lv, Y. Huang, L. Hao, X. Zhou, M. Xi, X. Tu *et al.*, *Phys. Rev. Appl.* **8**, 054005 (2017).
- ⁶²Y. Huang, H. Sun, D. An, X. Zhou, M. Ji, F. Rudau, R. Wieland, J. S. Hampp, O. Kizilaslan, J. Yuan *et al.*, *Phys. Rev. Appl.* **8**, 054023 (2017).
- ⁶³C. Watanabe, H. Minami, T. Kitamura, Y. Saiwai, Y. Shibano, T. Katsuragawa, H. Kubo, K. Sakamoto, T. Kashiwagi, R. A. Klemm, and K. Kadowaki, *Supercond. Sci. Technol.* **29**, 065022 (2016).
- ⁶⁴X. Zhou, Q. Zhu, M. Ji, D. An, L. Hao, H. Sun, S. Ishida, F. Rudau, R. Wieland, J. Li *et al.*, *Appl. Phys. Lett.* **107**, 122602 (2015).
- ⁶⁵X. J. Zhou, J. Yuan, H. Wu, Z. S. Gao, M. Ji, D. Y. An, Y. Huang, F. Rudau, R. Wieland, B. Gross *et al.*, *Phys. Rev. Appl.* **3**, 044012 (2015).
- ⁶⁶T. Kashiwagi, T. Tanaka, C. Watanabe, H. Kubo, Y. Komori, T. Yuasa, Y. Tanabe, R. Ota, G. Kuwano, K. Nakamura *et al.*, *J. Appl. Phys.* **122**, 233902 (2017).
- ⁶⁷L. N. Bulaevskii and A. E. Koshelev, *Phys. Rev. Lett.* **99**, 057002 (2007).
- ⁶⁸S. Lin and X. Hu, *Phys. Rev. Lett.* **100**, 247006 (2008).
- ⁶⁹X. Hu and S. Lin, *Phys. Rev. B* **78**, 134510 (2008).
- ⁷⁰A. E. Koshelev and L. N. Bulaevskii, *Phys. Rev. B* **77**, 014530 (2008).
- ⁷¹A. E. Koshelev, *Phys. Rev. B* **78**, 175409 (2008).
- ⁷²M. Tachiki, S. Fukuya, and T. Koyama, *Phys. Rev. Lett.* **102**, 127002 (2009).
- ⁷³M. Machida, Y. Ota, N. Sasa, T. Koyama, and H. Matsumoto, *J. Phys. Conf. Ser.* **248**, 012037 (2010).
- ⁷⁴A. E. Koshelev, *Phys. Rev. B* **82**, 174512 (2010).
- ⁷⁵R. A. Klemm and K. Kadowaki, *J. Supercond. Nov. Magn.* **23**, 613 (2010).
- ⁷⁶R. A. Klemm and K. Kadowaki, *J. Phys.: Condens. Matter* **22**, 375701 (2010).
- ⁷⁷V. M. Krasnov, *Phys. Rev. B* **83**, 174517 (2011).
- ⁷⁸A. A. Yurgens, *Phys. Rev. B* **83**, 184501 (2011).
- ⁷⁹R. A. Klemm, E. R. LaBerge, D. R. Morley, T. Kashiwagi, M. Tsujimoto, and K. Kadowaki, *J. Phys.: Condens. Matter* **23**, 025701 (2011).
- ⁸⁰B. Gross, S. Guénon, J. Yuan, M. Y. Li, J. Li, A. Ishii, R. G. Mints, T. Hatano, P. H. Wu, D. Koelle, H. B. Wang, and R. Kleiner, *Phys. Rev. B* **86**, 094524 (2012).
- ⁸¹S. Z. Lin and X. Hu, *Phys. Rev. B* **86**, 054506 (2012).
- ⁸²H. Asai and S. Kawabata, *Appl. Phys. Lett.* **104**, 112601 (2014).
- ⁸³H. Asai and S. Kawabata, *Appl. Phys. Lett.* **110**, 132601 (2017).
- ⁸⁴D. P. Cerkoney, C. Reid, C. M. Doty, A. Gramajo, T. D. Campbell, M. A. Morales, K. Delfanazari, M. Tsujimoto, T. Kashiwagi, T. Yamamoto *et al.*, *J. Phys.: Condens. Matter* **29**, 015601 (2017).
- ⁸⁵R. A. Klemm, A. E. Davis, and Q. X. Wang, *IEEE J. Sel. Top. Quantum Electron.* **23**, 8501208 (2017).
- ⁸⁶R. A. Klemm, A. E. Davis, Q. X. Wang, T. Yamamoto, D. P. Cerkoney, C. Reid, M. L. Koopman, H. Minami, T. Kashiwagi, J. R. Rain *et al.*, *IOP Conf. Ser.: Mater. Sci. Eng.* **279**, 012017 (2017).
- ⁸⁷U. Welp, K. Kadowaki, and R. Kleiner, *Nat. Photonics* **7**, 702 (2013).
- ⁸⁸I. Takeya and H. B. Wang, *Supercond. Sci. Technol.* **29**, 073001 (2016).
- ⁸⁹T. Kashiwagi, H. Kubo, K. Sakamoto, T. Yuasa, Y. Tanabe, C. Watanabe, T. Tanaka, Y. Komori, R. Ota, G. Kuwano *et al.*, *Supercond. Sci. Technol.* **30**, 074008 (2017).
- ⁹⁰T. Mochiku and K. Kadowaki, *Physica C* **235-240**, 523 (1994).
- ⁹¹T. Mochiku, K. Hirata, and K. Kadowaki, *Physica C* **282-287**, 475 (1997).